Supporting Information

Efficient productions of 5-hydroxymethylfurfural and alkyl levulinate from biomass carbohydrate using ionic liquid-based polyoxometalate salts

Jinzhu Chen,*[a] Guoying Zhao[a] and Limin Chen[b]

[a] *CAS Key Laboratory of Renewable Energy, Guangzhou Institute of Energy Conversion, Chinese Academy of Sciences, Guangzhou 510640, PR China*
[b] *Guangdong Provincial Key Laboratory of Atmospheric Environment and Pollution Control, College of Environment and Energy, South China University of Technology, Guangzhou 510006, PR China*
* *Corresponding author. Tel./Fax: (+86)-20-3722-3380. E-mail address: chenjz@ms.giec.ac.cn (J. Chen)*

Keywords: Biomass carbohydrate, Ethyl levulinate, 5-Hydroxymethylfurfural, ionic liquid-based polyoxometalate, Solid acid

1. Experimental

1.1. Procedure for the catalyst preparation

The ILs **3**–**7** were prepared according to literature procedure with slight modifications (Scheme 2). In a typical synthetic procedure of **3**, to a solution of TMEDA (2.9 g, 25 mmol) in ethanol (5 mL) was portion-wise added 1,3-propanesulfonate (6.1 g, 50 mmol) within 15 minutes. The mixture was then stirred under a nitrogen atmosphere for 2 hours at 60 °C. The reaction system was cooled to room temperature; the white precipitate thus formed was isolated by filtration, and washed with ethyl acetate (3×50 mL) then dried under vacuum. IL **3** was obtained as white solid with the yield of 91%. **3**: ^{1}H NMR (400 MHz, D_2O): δ = 3.96 (s, 4H), 3.59 (m, 4H), 3.24 (s, 12H), 2.98 (t, 4H, *J* = 8.0 Hz), 2.27 (m, 4H).[1]

Preparation of **4**: **4** was prepared by refluxing 4,4′-bipyridine (0.78 g, 5.0 mmol) with 1,3-propanesultone (1.5 g, 12 mmol) for 15 minutes at 120 °C without solvent under a nitrogen atmosphere. To the resulting semi-solid mixture, dimethyl sulfoxide (5 mL) was injected and heated at 120 °C while being stirred continuously for 3 hours. After cooling, the white precipitate was filtered and washed several times with methanol, dried over filter papers to give 77% yield of the desired product of **4**, brown solid. **4**: ^{1}H NMR (400 MHz, D_2O): δ = 9.12 (d, 4H, *J* = 8.0 Hz), 8.53 (d, 4H, *J* = 8.0 Hz), 4.86 (t, 4H, *J* = 8.0 Hz), 2.99 (t, 4H, *J* = 6.0 Hz), 2.50 (m, 4H).[2]

Preparation of sodium salt of **5**: Sodium ethoxide (1.7 g, 25 mmol) and 2-methylimidazole (2.1 g, 25 mmol) were mixed in ethanol (5 mL) under a nitrogen atmosphere for 2 hours at room temperature. After that, an excess of 1,3-propanesultone (7.7 g, 63 mmol) was added to the mixture, and this solution was stirred for 2 hours at room temperature. The product was washed twice with ethanol, and then the precipitate was recovered and dried in a vacuum at 60 °C to give 74% yield of the desired product of sodium salt of **5**, white solid. [Na^+·**5**$^-$]: ^{1}H NMR (400 MHz, D_2O): δ = 7.39 (s, 2H), 4.22 (t, 4H, *J* = 8.0 Hz), 2.89 (t, 4H, *J* = 8.0 Hz), 2.58 (s, 3H), 2.19 (m, 4H).[3]

Preparation of **6**: 1-Methylimidazole (2.1 g, 25 mmol) and 1,3-propanesulfone (6.1 g, 25 mmol) were dissolved in toluene (5 mL) and stirred for 24 hours at 50 °C under a nitrogen atmosphere. A white precipitate formed which was filtered, washed with diethyl ether three times, and then dried in a vacuum at 60 °C to give 89% yield of the desired product of **6**, white solid. **6**: ^{1}H NMR (400 MHz, D_2O): δ = 8.71 (s, 1H), 7.48 (s, 1H), 7.41 (s, 1H), 4.32 (t, 2H, *J* = 8.0 Hz), 3.85 (s, 3H), 2.88 (t, 2H, *J* = 8.0 Hz), 2.27 (m, 2H).[4]

Preparation of **7**: Triphenylphosphine (6.6 g, 25 mmol) and 1,3-propanesultone (6.1 g, 25 mol) were combined in toluene (5 mL) and brought to reflux. Overnight, a white precipitate forms which is isolated by filtration and dried in a vacuum at 60 °C to give 80% yield of the desired product of **7**, white solid. **7**: ^{1}H NMR (400 MHz, D_2O): δ = 7.80–7.59 (m, 15H), 3.41 (m, 2H), 2.97 (t, 2H, *J* = 8.0 Hz), 2.05 (m, 2H).[5]

2. Results and Discussion

2.1. FTIR comparison of IL-POMs

Scheme 2 shows the structures of IL-POMs in this research. Generally, the ILs

3–**7** were prepared according to literature methods; whereas, the IL-POMs used in this research were prepared by the treatment of propane sulfonate-functionalized ILs **3**–**7** with HPA in water.

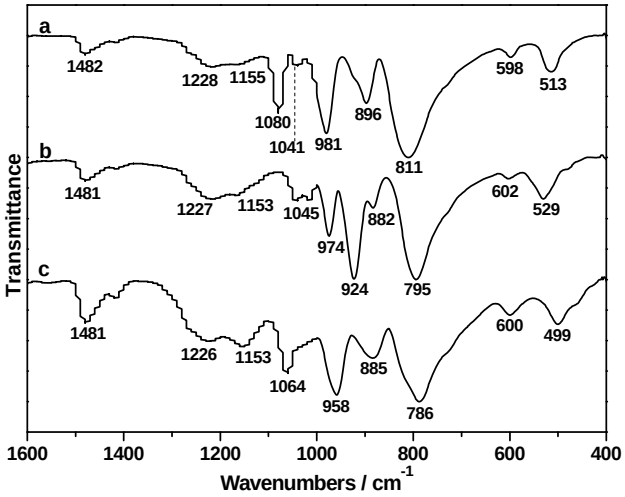

Figure S1. FT-IR of (a) $[\mathbf{3}\cdot 2H]_3[PW_{12}O_{40}]_2$, (b) $[\mathbf{3}\cdot 2H]_2[SiW_{12}O_{40}]$, and (c) $[\mathbf{3}\cdot 2H]_3[PMo_{12}O_{40}]_2$.

FT-IR spectra of $[\mathbf{3}\cdot 2H]_3[PW_{12}O_{40}]_2$, $[\mathbf{3}\cdot 2H]_2[SiW_{12}O_{40}]$, and $[\mathbf{3}\cdot 2H]_3[PMo_{12}O_{40}]_2$ were compared in Figure S1. The FT-IR spectra of **3**-POM hybrid samples clearly showed the presence of both the $[\mathbf{3}\cdot 2H]^{2+}$ and heteropolyanion species. In the case of $[\mathbf{3}\cdot 2H]_3[PW_{12}O_{40}]_2$, the band at 1482 cm^{-1} was attributed to the asymmetric deformation vibration of the C–H bond in CH_3 of **3** (Figure S1a).[6] In addition, two bands at 1228 and 1155 cm^{-1} were assigned to S=O stretching vibrations, indicating the presence of a sulfonic group.[7] The characteristic bands of $P–O_a$ vibration in $[\mathbf{3}\cdot 2H]_3[PW_{12}O_{40}]_2$ is visible at 1080 and 1041 cm^{-1}.[8,9] While, the vibration of $W=O_d$ stretching appears at 981 cm^{-1}. Vibrations associated with $W–O_b–W$ and $W–O_c–W$, are observed at 896 and 811 cm^{-1}, respectively (Figure S1a).

For FT-IR spectra of $[\mathbf{3}\cdot 2H]_2[SiW_{12}O_{40}]$, the bands at 1045 and 924 cm^{-1} are assigned to stretching vibration of $Si–O_a$, while the peak at 974 cm^{-1} can be indexed to terminal bands vibration of $W=O_d$. Vibrations associated with $W–O_b–W$ and $W–O_c–W$, are observed at 882 and 795 cm^{-1}, respectively (Figure S1b).[8,9] In the case of $[\mathbf{3}\cdot 2H]_3[PMo_{12}O_{40}]_2$, the peaks at 1064 and 958 cm^{-1} can be assigned to stretching vibration of $P–O_a$ and terminal bands vibration of $Mo=O_d$, respectively, while the bands at 786 cm^{-1} and 885 cm^{-1} are associated with stretching vibration of $Mo–O_c–Mo$ and $Mo–O_b–Mo$, respectively (Figure S1c).[8,9] The above FT-IR spectra analysis thus confirmed the structure of **3**-POM hybrids.

2.2. The influence of solvent on fructose conversion

The influence of solvent on fructose conversion to HMF was also investigated under similar reaction conditions, different aprotic (DMSO, DMF and THF), and protic (alcohols) solvents were employed with $[\mathbf{3}\cdot 2H]_3[PW_{12}O_{40}]_2$ as catalyst (Table

S1, Runs 1–6). The yield of HMF with DMSO, achieving 90% with a full fructose conversion (Table S1, Run 1), was much higher than that with the other solvents. On the contrary, the conversion of fructose dehydration with *iso*-butanol as slovent is remarkably inferior, producing HMF yield only of 10%. Furthermore, the catalyst $[\mathbf{3}\cdot 2H]_3[PW_{12}O_{40}]_2$ is insoluble in the solvents described in table S1, precipitates at the end of the reaction and can be easily recycled.

Table S1. Conversion of fructose into HMF in various solvents and the influence of the solvent volume[a]

Run	Solvent	Volume [mL]	Conversion [%]	Yield [%]
1	DMSO	2	>99	90
2	DMF	2	89	49
3	THF	2	99	25
4	iso-Propanol	2	89	35
5	sec-Butanol	2	74	16
6	iso-Butanol	2	68	10
7	DMSO	1	>99	84
8	DMSO	3	99	89
9	DMSO	4	99	88
10	DMSO	5	98	86

[a] Reaction conditions: fructose (50 mg, 0.28 mmol), $[\mathbf{3}\cdot 2H]_3[PW_{12}O_{40}]_2$, (25 mg, 2.5 mol%), 100 °C, 0.5 h.

2.3. The influence of fructose concentration on its conversion

It has been pointed out that the carbohydrate concentration affected the HMF yield in acidic medium. For higher fructose concentrations, the HMF yield decreases due to the formation of larger amounts of humins. Consequently, the fructose dehydration reaction with $[\mathbf{3}\cdot 2H]_3[PW_{12}O_{40}]_2$ as solid acid catalyst was performed by changing the amount of DMSO to investigate the effect of the fructose concentrations on HMF yields. When using 1 mL of DMSO, the yield of HMF was 84% which was lower than that obtained with 2 mL of DMSO with HMF yield of 90% at the same reaction time point (Table 2, Runs 1 and 7). Furthermore, during the reaction process, the reaction system quickly turned dark brown in 1 mL of DMSO. This indicated that HMF readily further polymerized to form oligomers under the relatively high concentration. By further increasing the DMSO volume to 3 mL, 4 mL and 5 mL, HMF yields, however, decreased with fructose concentration.

References

[1] D. Fang, J.M. Yang, C.M. Jiao, ACS Catalysis 1 (2011) 42–47.
[2] S. Bhandari, M. Deepa, S. Pahal, A.G. Joshi, A.K. Srivastava, R. Kant, ChemSusChem 3 (2010) 97–105.
[3] Y. Masahiro, H. Ohno, Ionics 8 (2002) 267–271.
[4] Y. Leng, J. Wang, D.R. Zhu, X.Q. Ren, H.Q. Ge, L. Shen, Angewandte Chemie

121 (2008) 174–177; Angewandte Chemie International Edition 48 (2008) 168–171.
[5] A.C. Cole, J.L. Jensen, I. Ntai, K.L.T. Tran, K.J. Weaver, D.C. Forbes, J.H. Davis, Jr., Journal of the American Chemical Society, 124 (2002) 5962–5963.
[6] G. Socrates, Infrared and Raman Characteristic Group Frequencies, Tables and Charts, 3rd ed., J. Wiley & Sons, New York, 2001.
[7] Z.H. Zhang, K. Dong, Z.B. Zhao, ChemSusChem 4 (2011) 112–118.
[8] D.S. Pito, I. Matos, I.M. Fonseca, A.M. Ramos, J. Vital, J.E. Castanheiro, Applied Catalysis A: General 373 (2010) 140–146
[9] F. Chai, F.H. Cao, F.Y. Zhai, Y. Chen, X.H. Wang, Z.M. Su, Advanced Synthesis & Catalysis 349 (2007) 1057–1065.

Figure S2. ^{1}H and $^{13}C\{^{1}H\}$ NMR analysis.

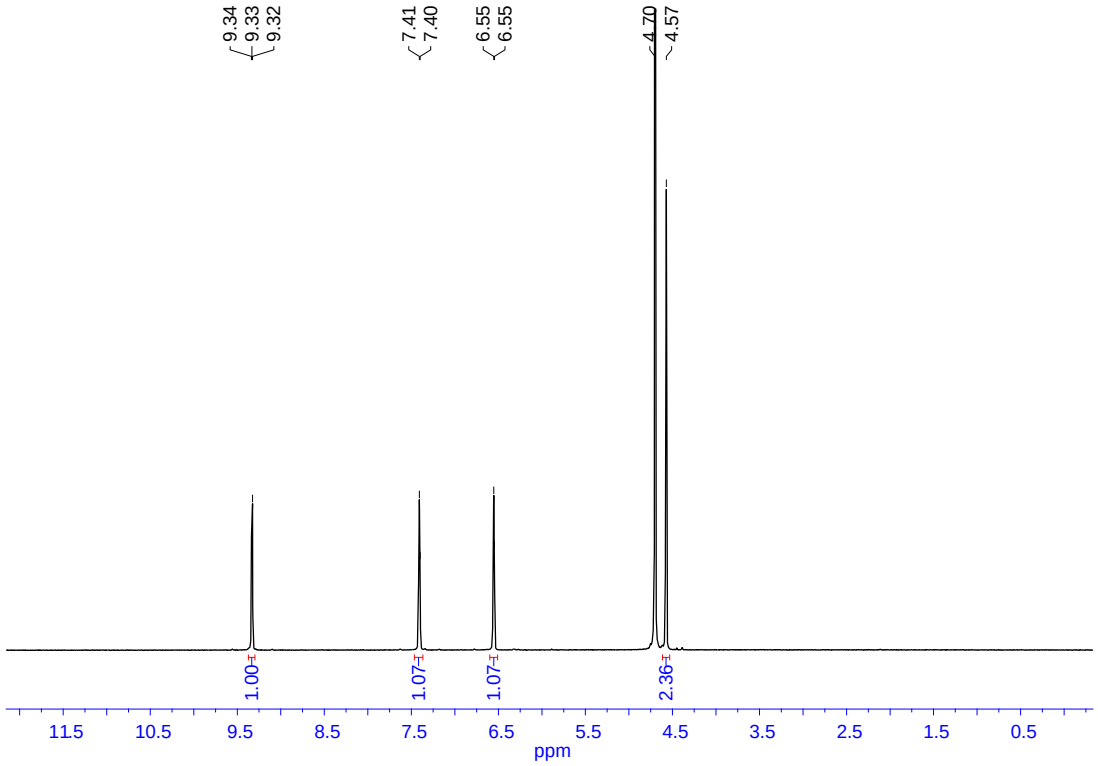

Figure S2-1. ^{1}H NMR of 5-hydroxymethylfurfural in D_2O.

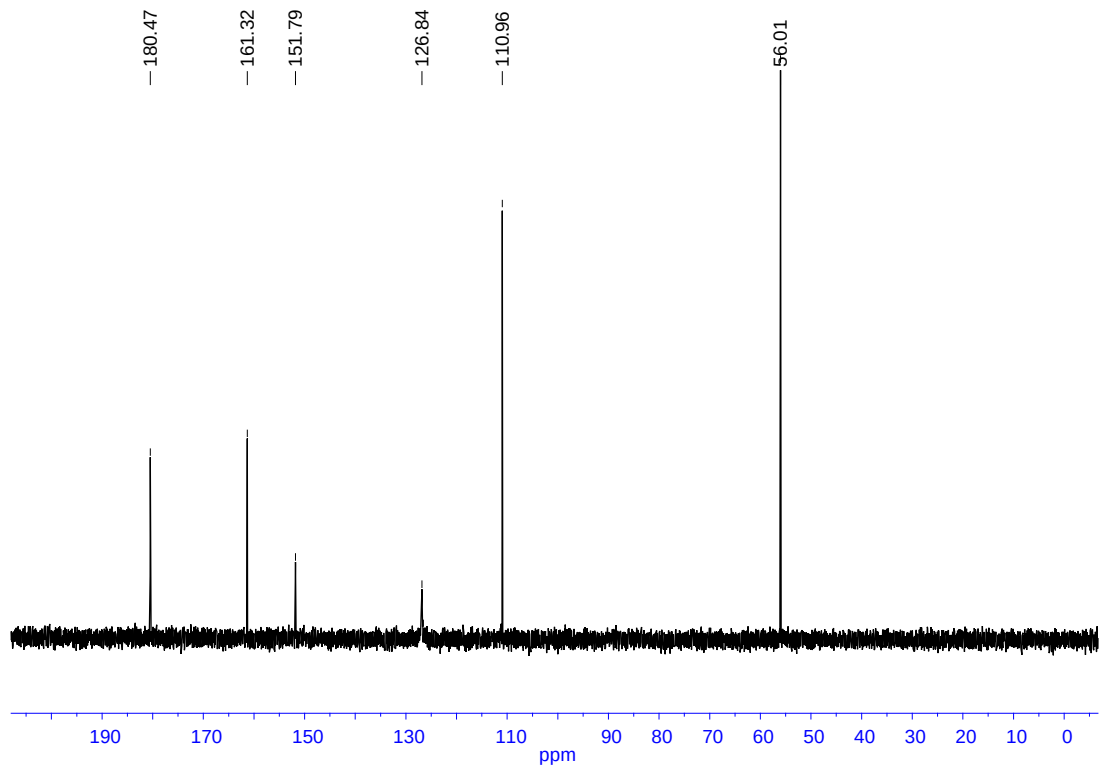

Figure S2-2. ^{13}C {^{1}H} NMR of 5-hydroxymethylfurfural in D_2O.

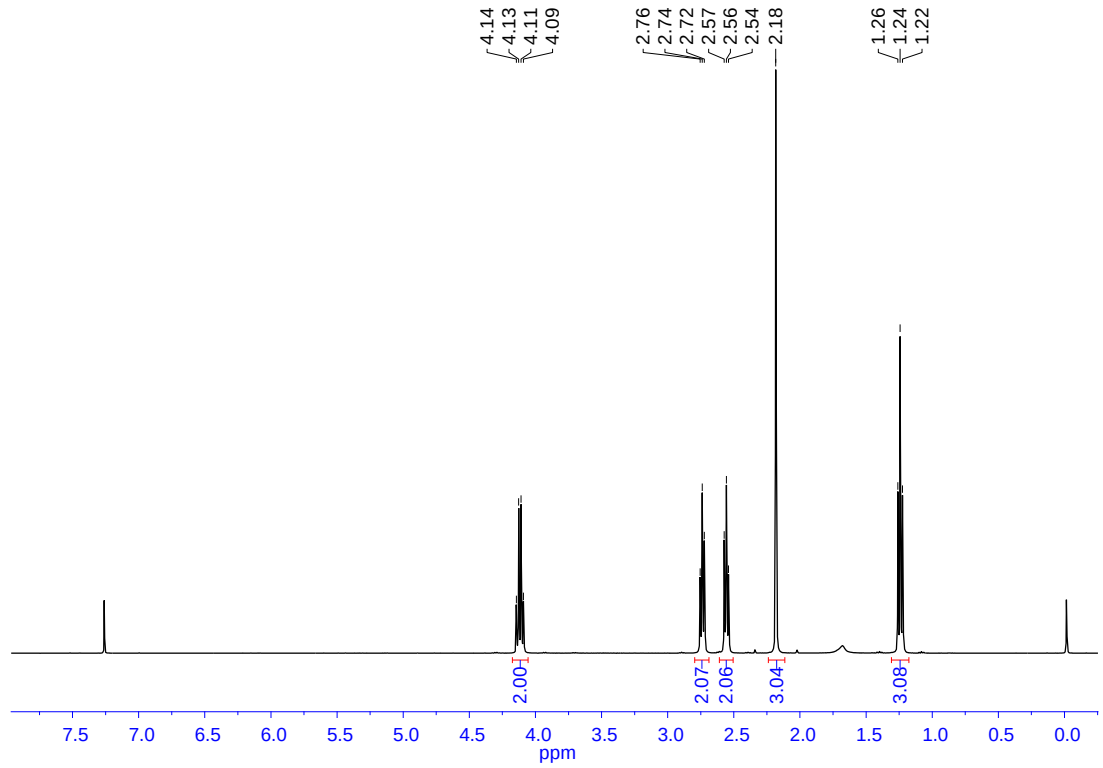

Figure S2-3. ^{1}H NMR of ethyl levulinate in $CDCl_3$.

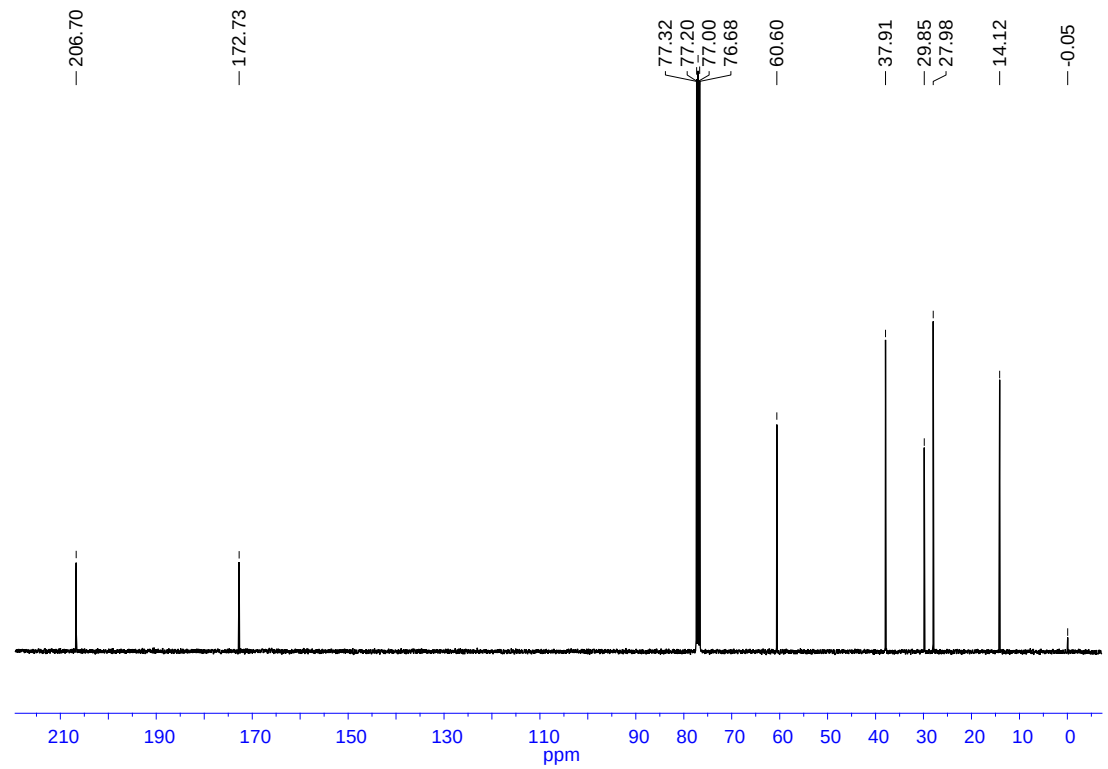

Figure S2-4. ^{13}C {^{1}H} NMR of ethyl levulinate in $CDCl_3$.

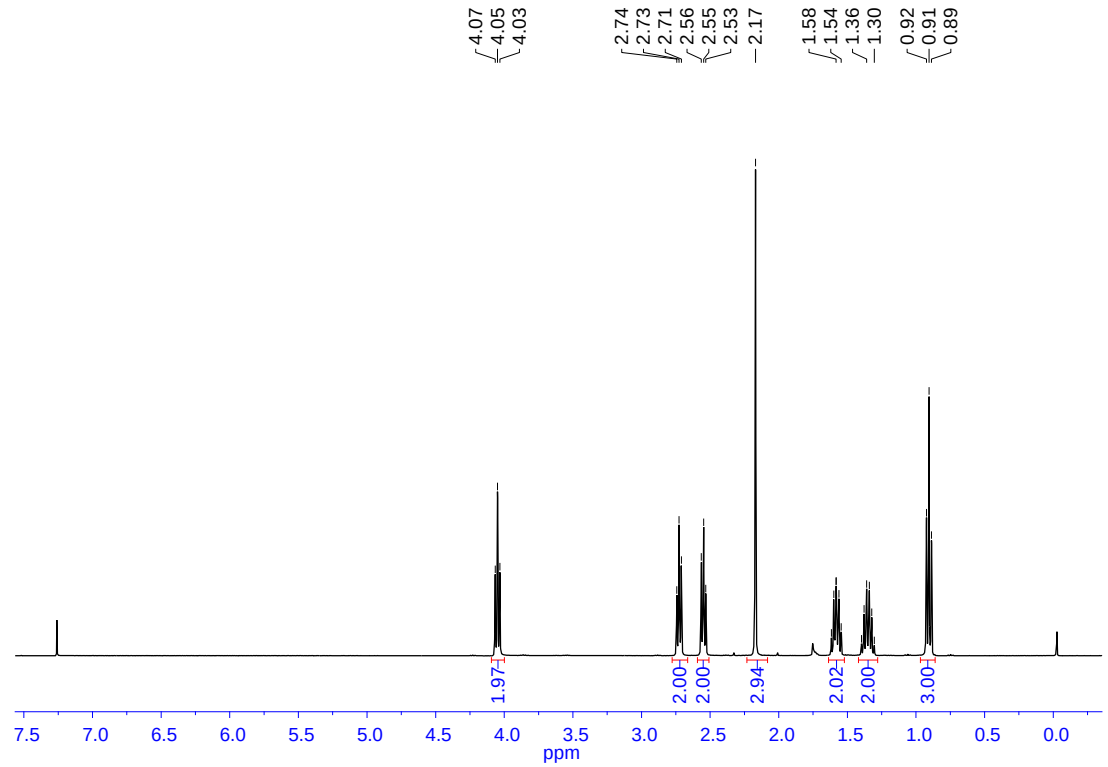

Figure S2-5. ^{1}H NMR of n-butyl levulinate in $CDCl_3$.

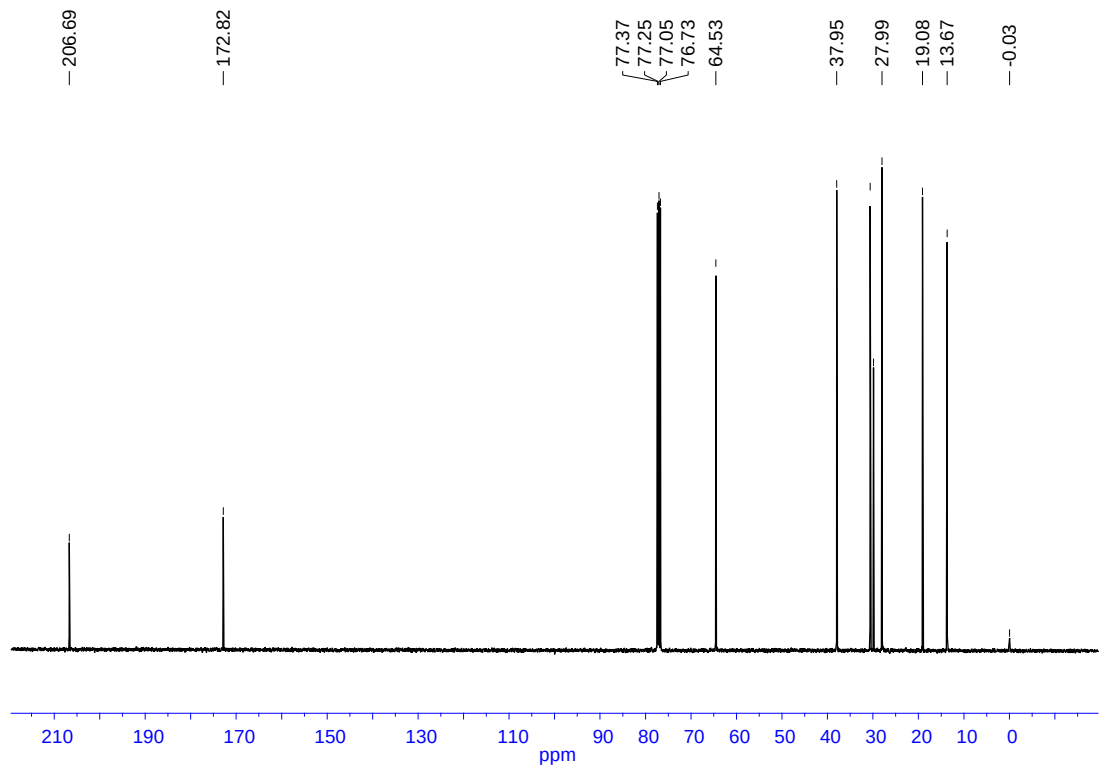

Figure S2-6. ^{13}C {^{1}H} NMR of n-butyl levulinate in $CDCl_3$.

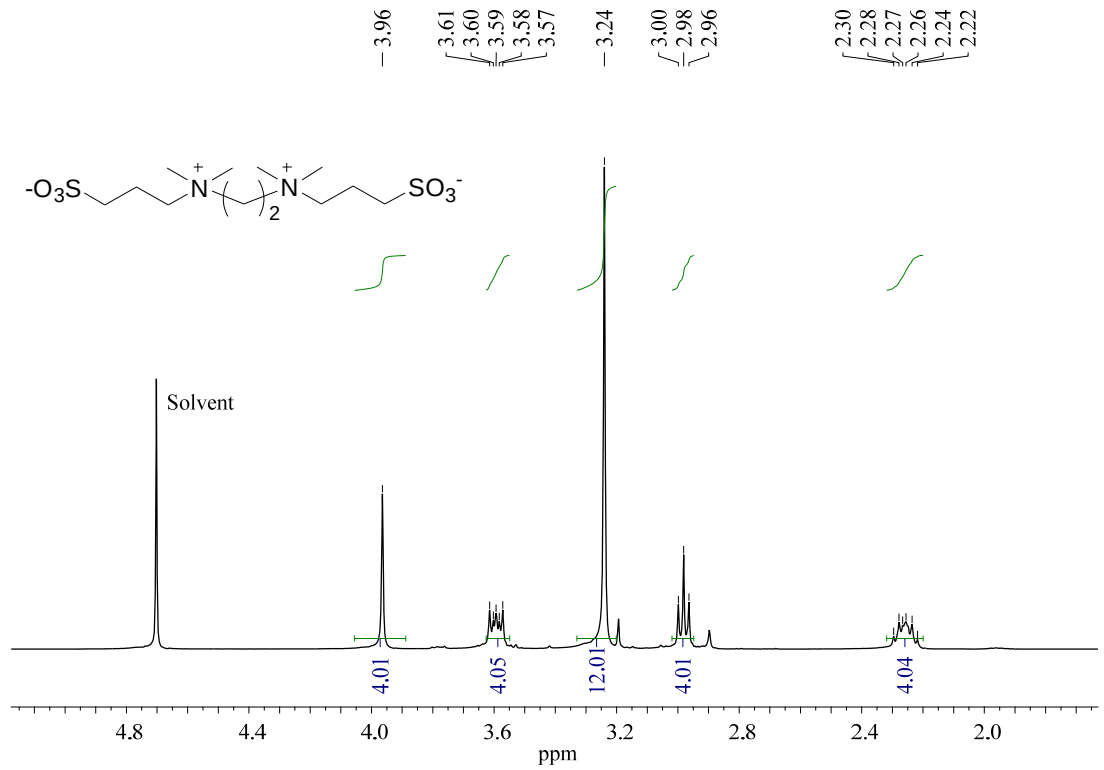

Figure S2-7. ^{1}H NMR of **3** in D_2O.

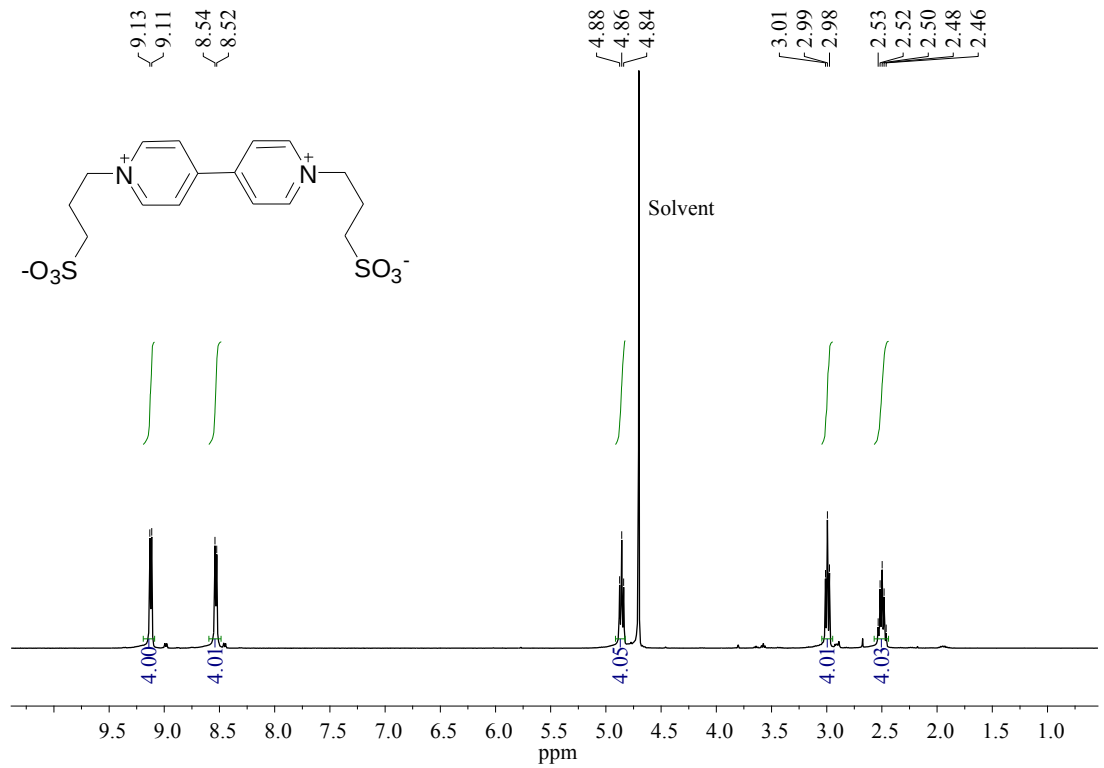

Figure S2-8. ^{1}H NMR of **4** in D_2O

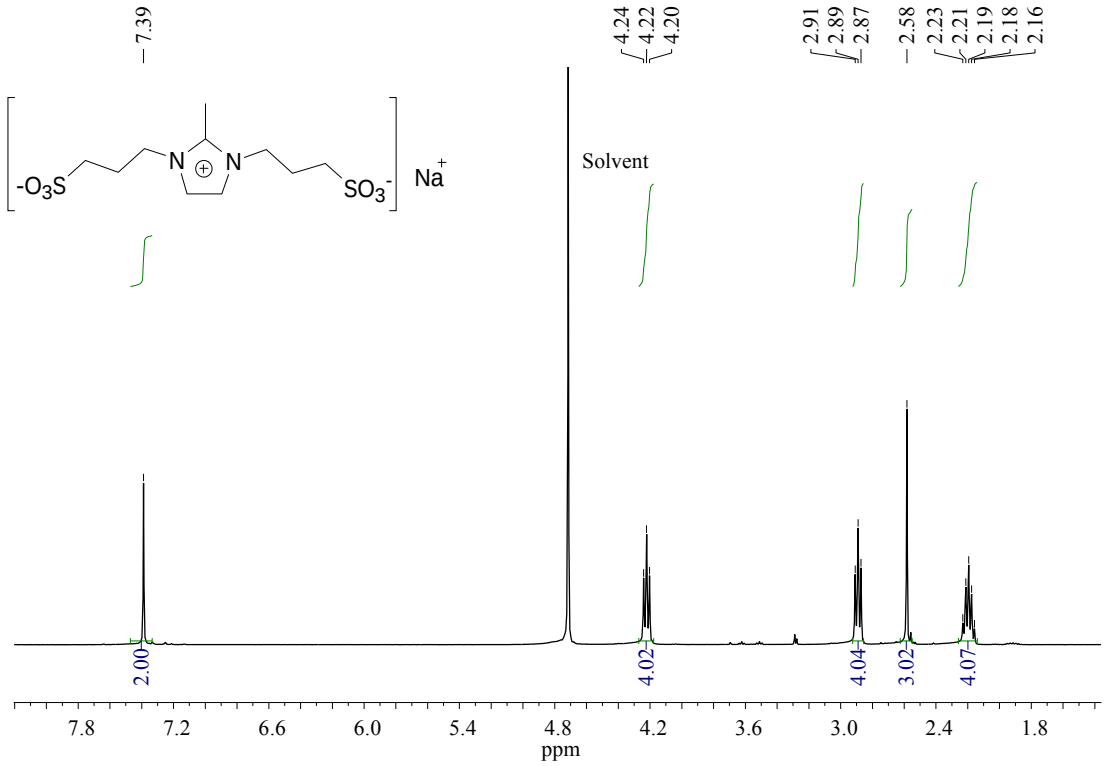

Figure S2-9. ^{1}H NMR of sodium salt of **5** in D_2O

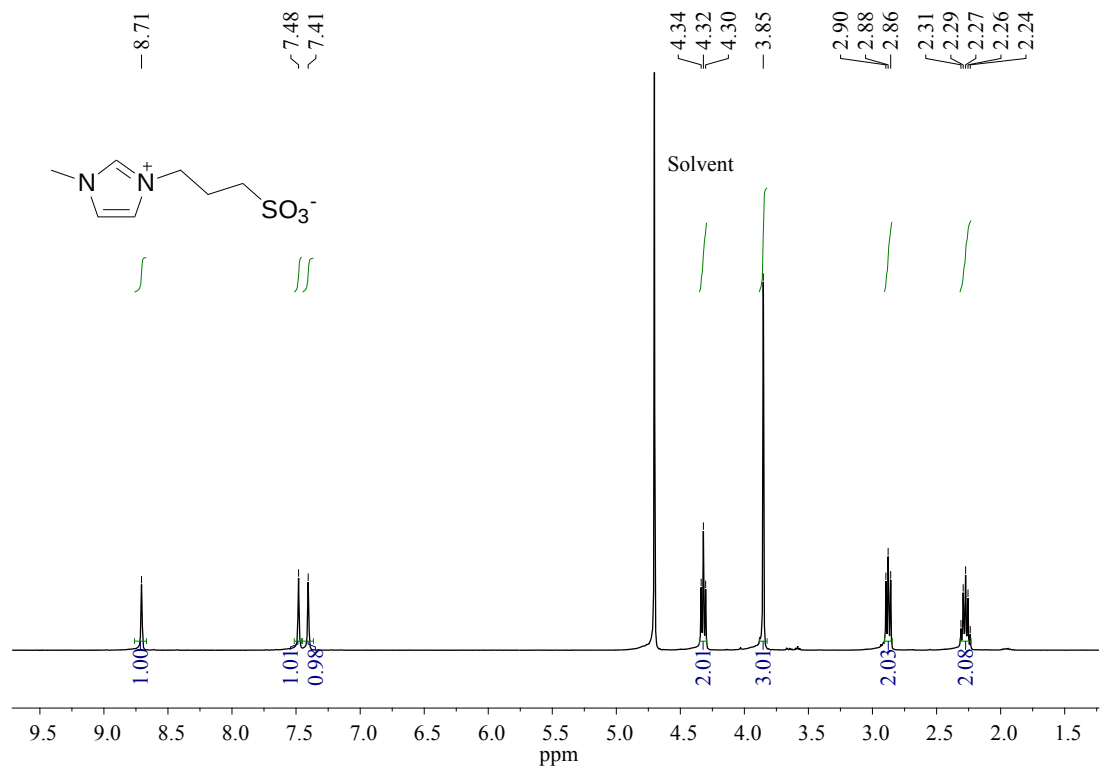

Figure S2-10. ^{1}H NMR of **6** in D_2O

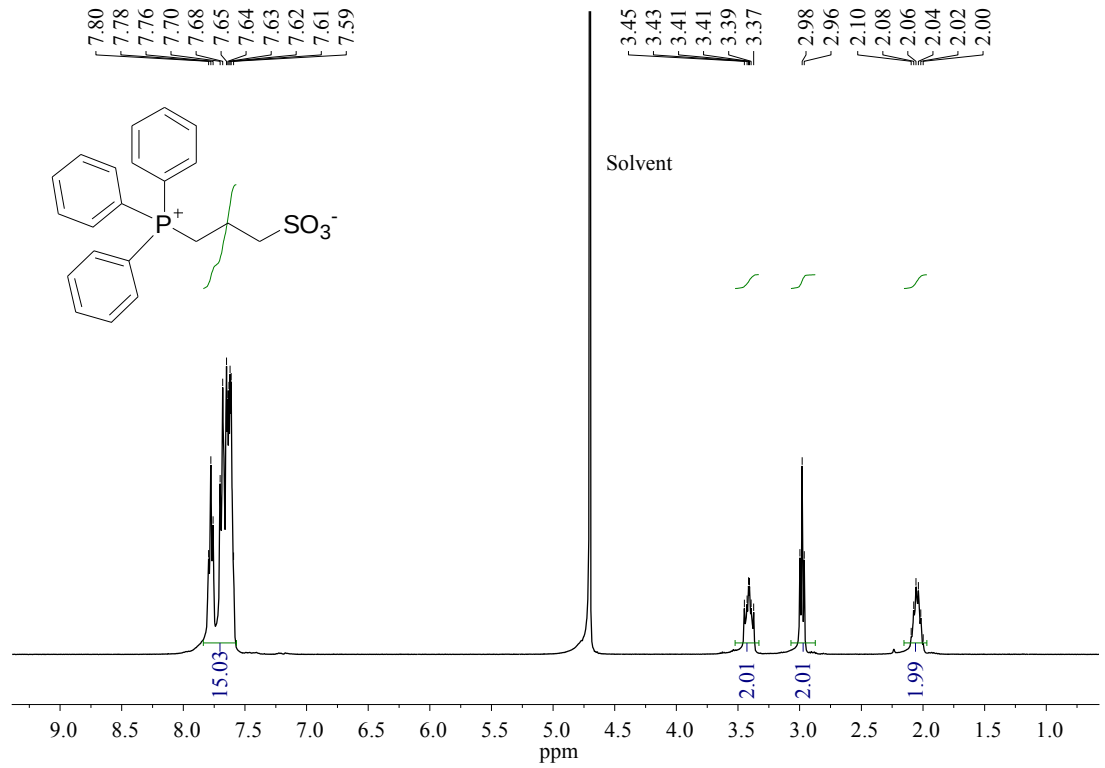

Figure S2-11. ^{1}H NMR of **7** in D_2O

Figure S3. FT-IR analysis

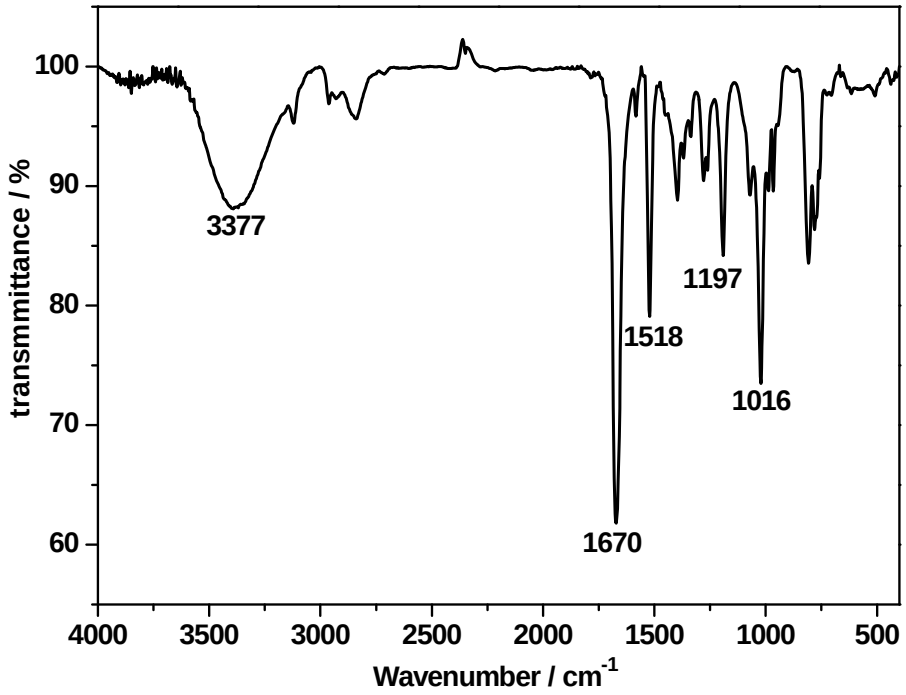

Figure S3-1. FT-IR of 5-hydroxymethylfurfural on KBr Pellet. FT-IR (KBr, cm^{-1}): ν = 3377 (O–H), 1670 (C=O).

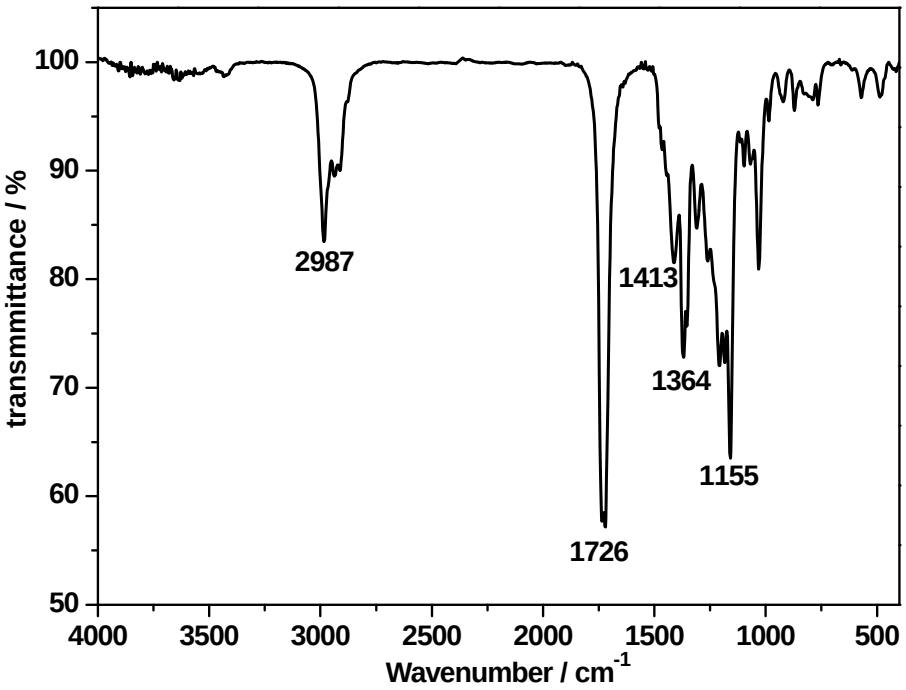

Figure S3-2. FT-IR of ethyl levulinate on KBr Pellet. FT-IR (KBr, cm^{-1}): ν = 1726 (C=O).

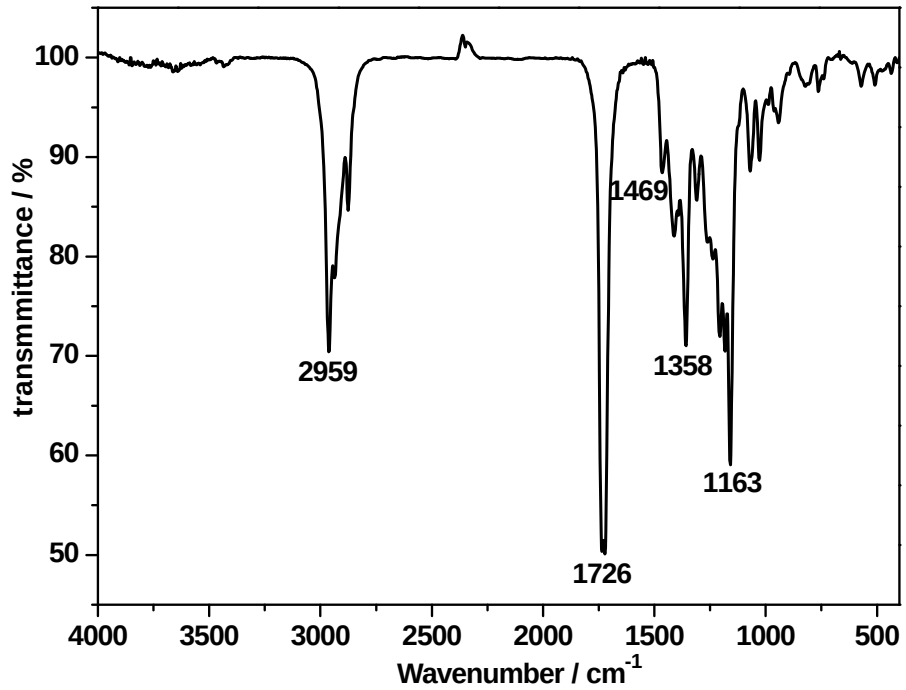

Figure S3-3. FT-IR of butyl levulinate on KBr Pellet. FT-IR (KBr, cm^{-1}): ν = 1726 (C=O).

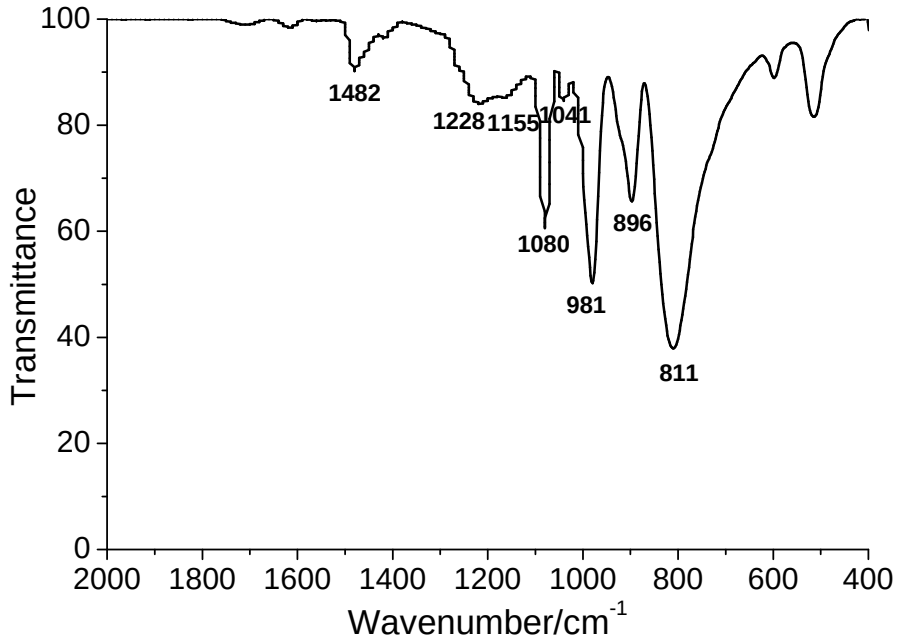

Figure S3-4. FT-IR of $[\mathbf{3}\cdot 2H]_3[PW_{12}O_{40}]_2$ on KBr Pellet. FT-IR (KBr, cm^{-1}): ν = 1482 (C–H in CH_3), 1228, 1155 (S=O), 1080, 1041 (P–O_a), 981 (W=O_d), 896 (W–O_b–W), 811 (W–O_c–W).

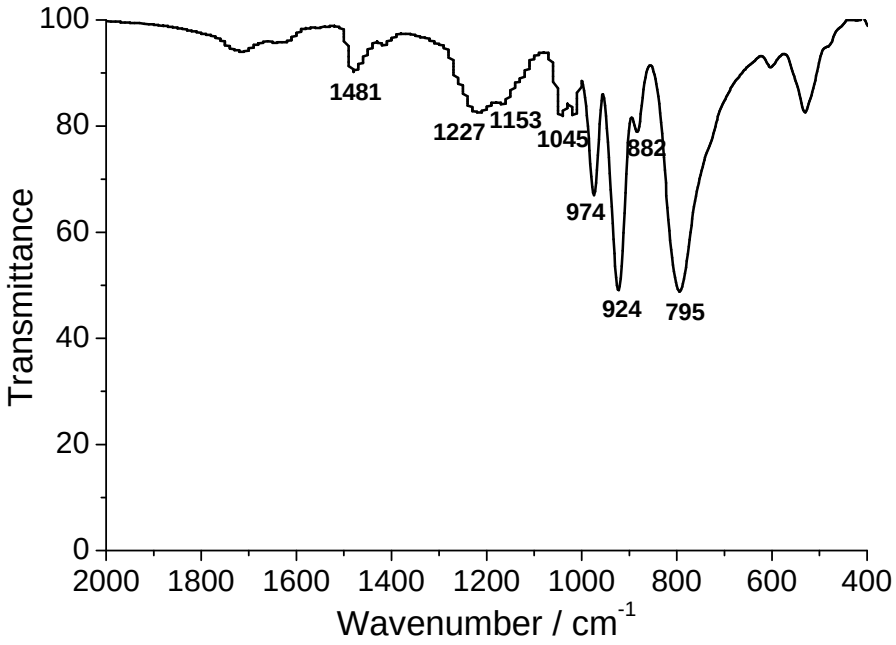

Figure S3-5. FT-IR of $[\mathbf{3}\cdot 2H]_2[SiW_{12}O_{40}]$ on KBr Pellet. FT-IR (KBr, cm^{-1}): ν = 1481 (C–H in CH_3), 1227, 1153 (S=O), 1045, 924 (Si–O_a), 974 (W=O_d), 882 (W–O_b–W), 795 (W–O_c–W).

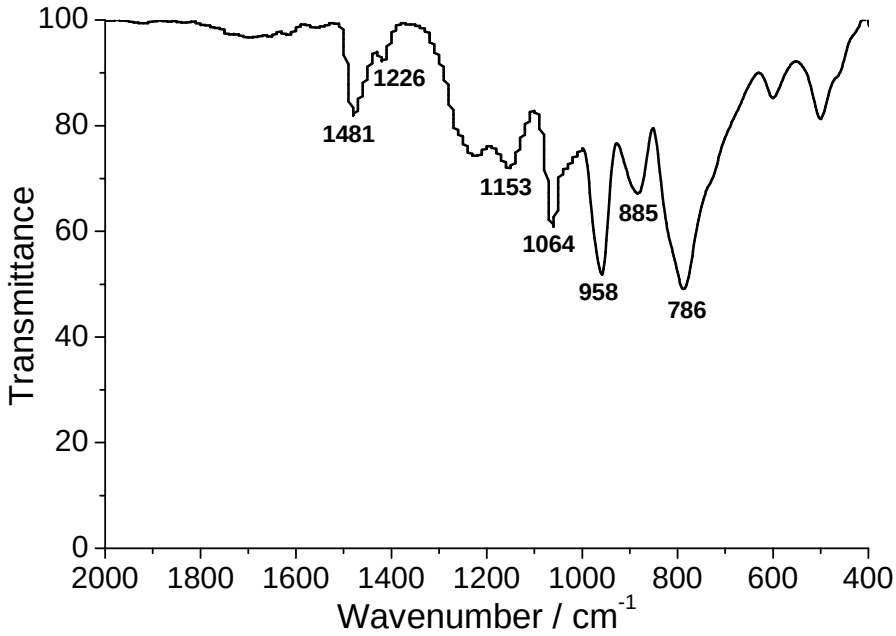

Figure S3-6. FT-IR of $[\mathbf{3}\cdot 2H]_3[PMo_{12}O_{40}]_2$ on KBr Pellet. FT-IR (KBr, cm^{-1}): ν = 1481 (C–H in CH_3), 1226, 1153 (S=O), 1064 (P–O_a), 958 (Mo=O_d), 885 (W–O_b–W), 786 (W–O_c–W).

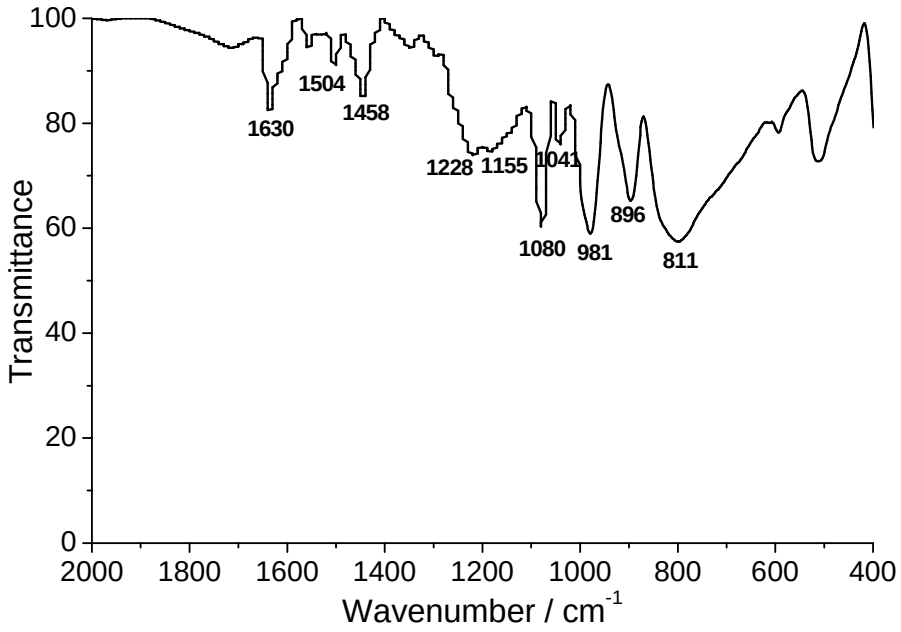

Figure S3-7. FT-IR of $[\mathbf{4}\cdot 2H]_3[PW_{12}O_{40}]_2$ on KBr Pellet. FT-IR (KBr, cm^{-1}): ν = 1630 (C=N, C–N), 1504, 1458 (C=C), 1228, 1155 (S=O), 1080, 1041 ($P–O_a$), 981 ($W=O_d$), 896 ($W–O_b–W$), 811 ($W–O_c–W$).

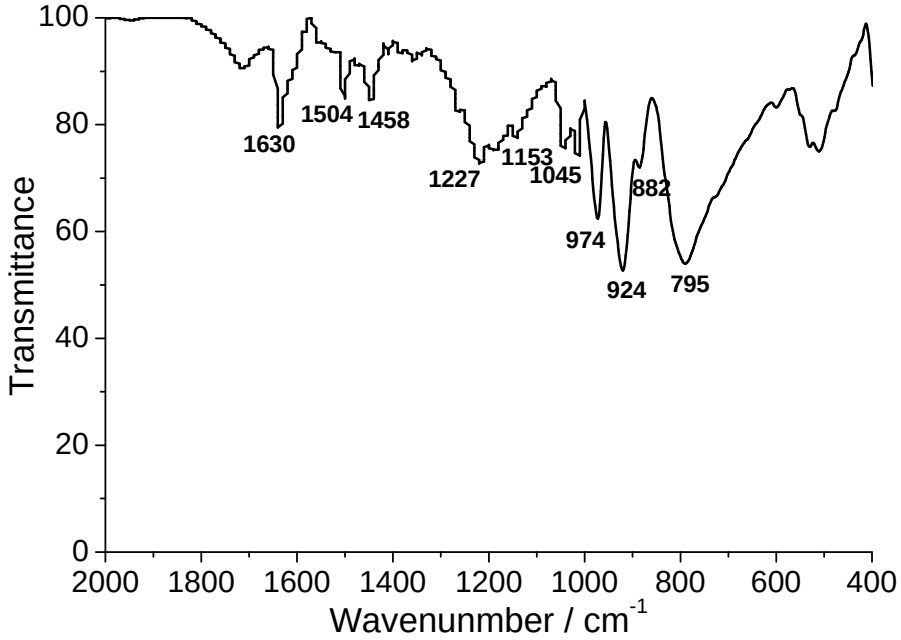

Figure S3-8. FT-IR of $[\mathbf{4}\cdot 2H]_2[SiW_{12}O_{40}]$ on KBr Pellet. FT-IR (KBr, cm^{-1}): ν = 1630 (C=N, C–N), 1504, 1458 (C=C), 1227, 1153 (S=O), 1045, 924 ($Si–O_a$), 974 ($W=O_d$), 882 ($W–O_b–W$), 795 ($W–O_c–W$)

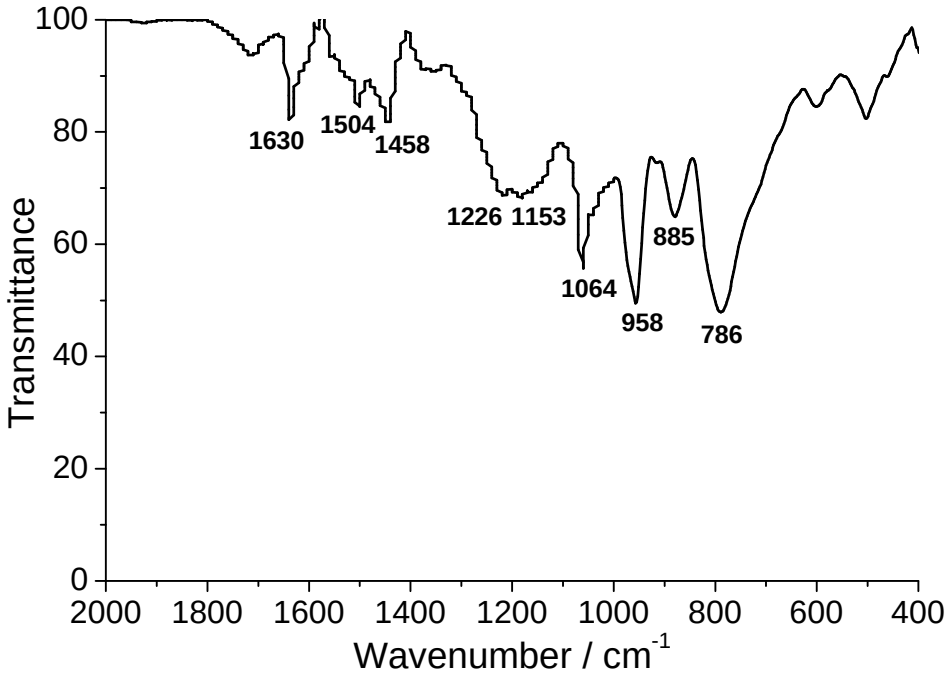

Figure S3-9. FT-IR of $[\mathbf{4}\cdot 2H]_3[PMo_{12}O_{40}]_2$ on KBr Pellet. FT-IR (KBr, cm^{-1}): ν = 1630 (C=N, C–N), 1504, 1458 (C=C), 1226, 1153 (S=O), 1064 (P–O_a), 958 (Mo=O_d), 885 (W–O_b–W), 786 (W–O_c–W).

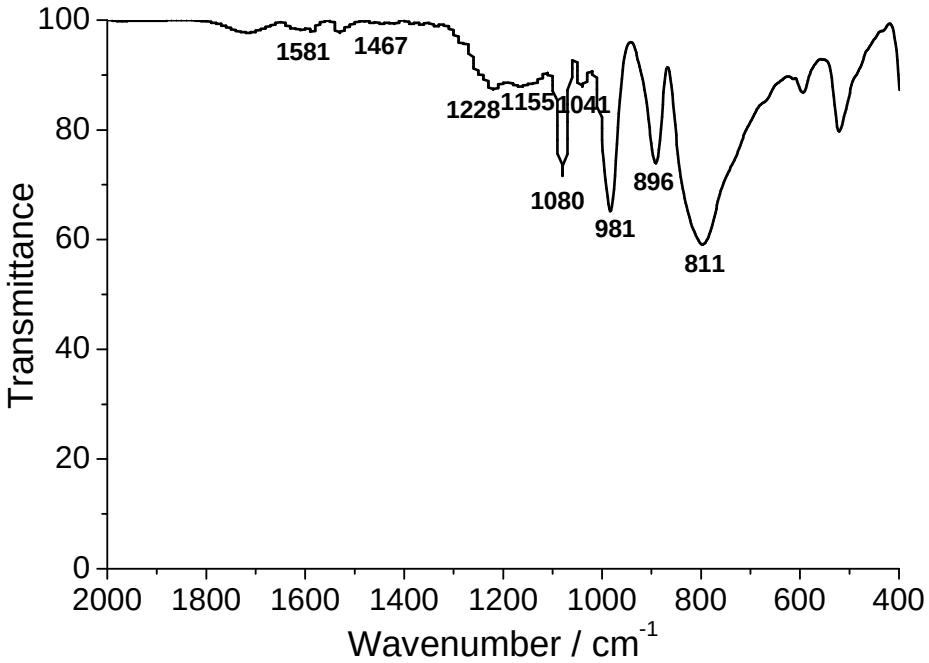

Figure S3-10. FT-IR of $[\mathbf{5}\cdot H]_3[PW_{12}O_{40}]$ on KBr Pellet. FT-IR (KBr, cm^{-1}): ν = 1581 (C=N), 1467 (C–H in CH_3), 1228, 1155 (S=O), 1080, 1041 (P–O_a), 981 (W=O_d), 896 (W–O_b–W), 811 (W–O_c–W).

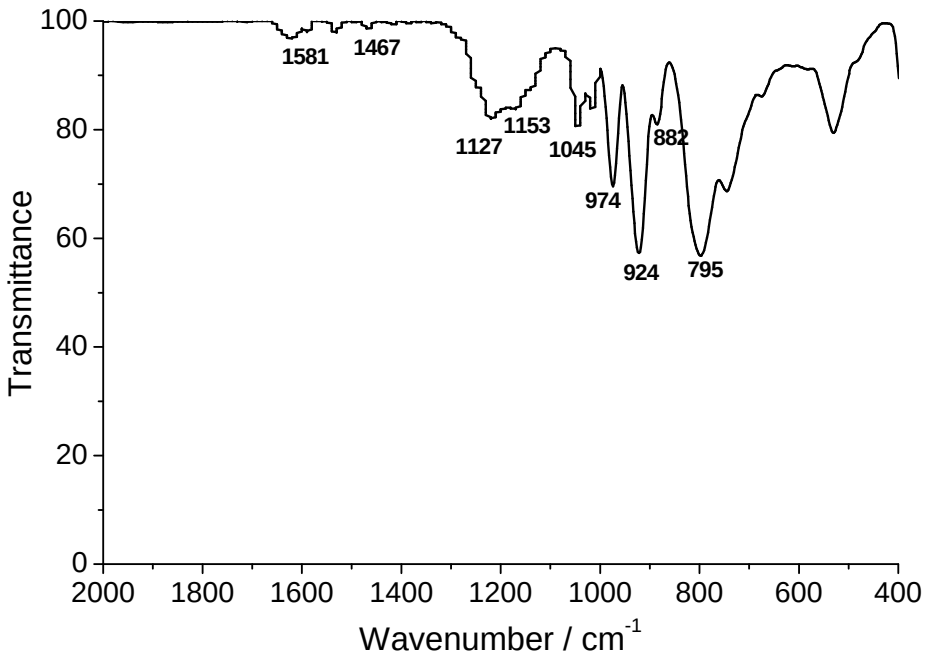

Figure S3-11. FT-IR of [**5**·H]$_4$[$SiW_{12}O_{40}$] on KBr Pellet. FT-IR (KBr, cm^{-1}): ν = 1581 (C=N), 1467 (C–H in CH_3), 1227, 1153 (S=O), 1045, 924 (Si–O_a), 974 (W=O_d), 882 (W–O_b–W), 795 (W–O_c–W).

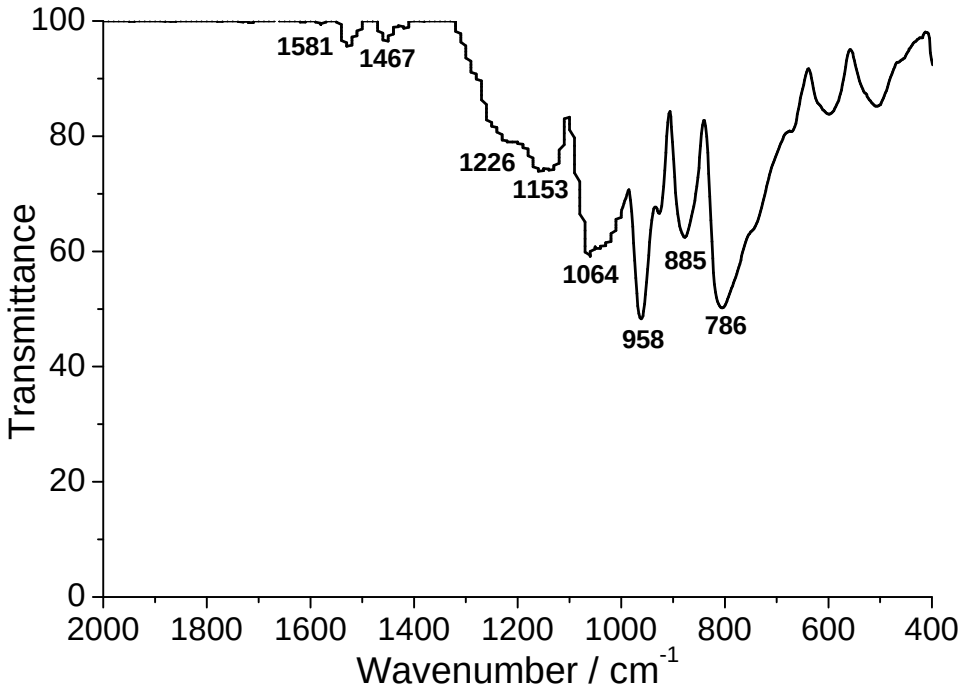

Figure S3-12. FT-IR of [**5**·H]$_3$[$PMo_{12}O_{40}$] on KBr Pellet. FT-IR (KBr, cm^{-1}): ν = 1581 (C=N), 1467 (C–H in CH_3), 1226, 1153 (S=O), 1064 (P–O_a), 958 (Mo=O_d), 885 (W–O_b–W), 786 (W–O_c–W).

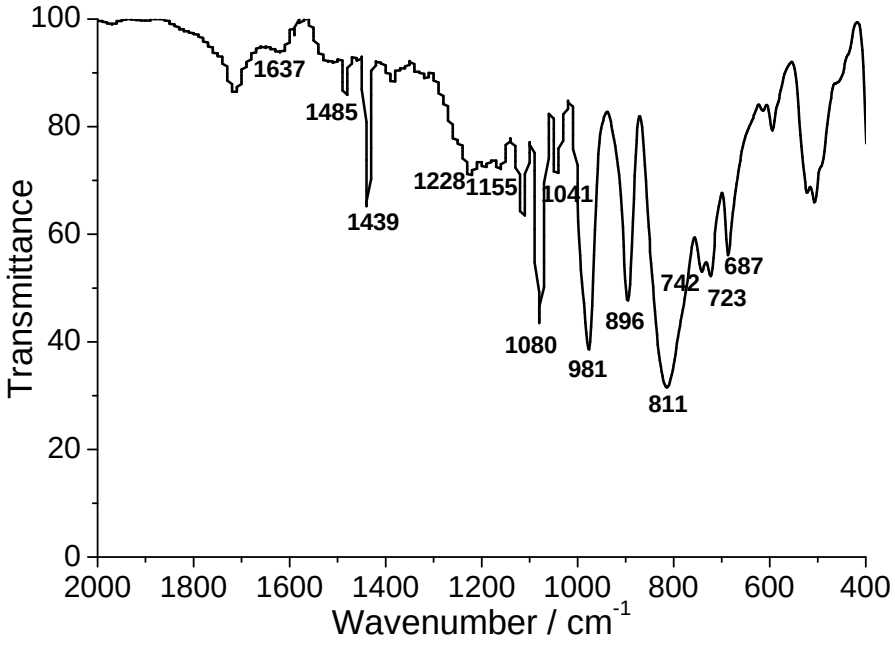

Figure S3-13. FT-IR of $[\mathbf{7}\cdot H]_3[PW_{12}O_{40}]$ on KBr Pellet. FT-IR (KBr, cm^{-1}): ν = 1637, 1485 (C=C), 723, 687 (C–H), 1439 (P–Ar), 742 (P–CH_2), 1228, 1155 (S=O), 1080, 1041 (P–O_a), 981 (W=O_d), 896 (W–O_b–W), 811 cm^{-1} (W–O_c–W).

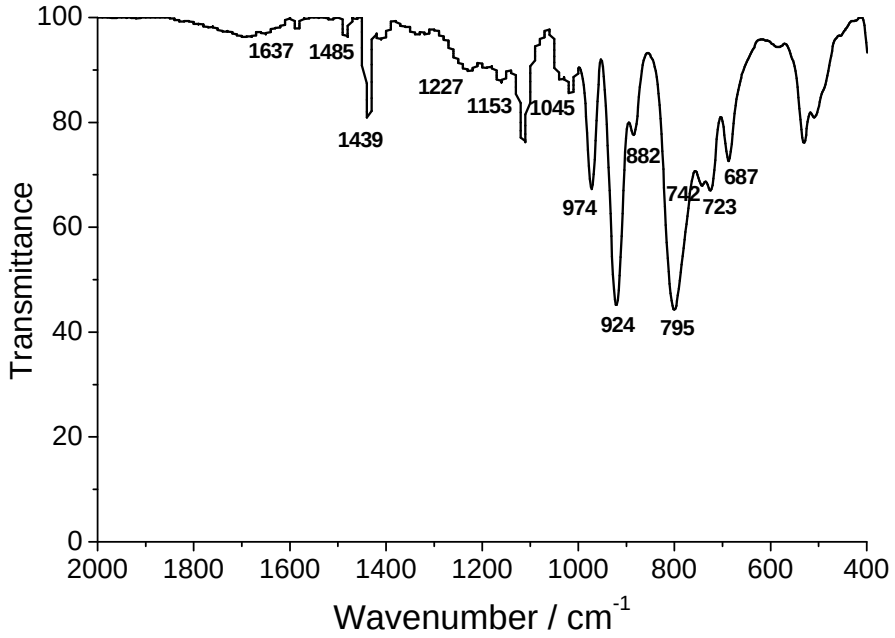

Figure S3-14. FT-IR of $[\mathbf{7}\cdot H]_4[SiW_{12}O_{40}]$ on KBr Pellet. FT-IR (KBr, cm^{-1}): ν = 1637, 1485 (C=C), 723, 687 (C–H), 1439 (P–Ar), 742 (P–CH_2), 1227, 1153 (S=O), 1045, 924 (Si–O_a), 974 (W=O_d), 882 (W–O_b–W), 795 cm^{-1} (W–O_c–W).

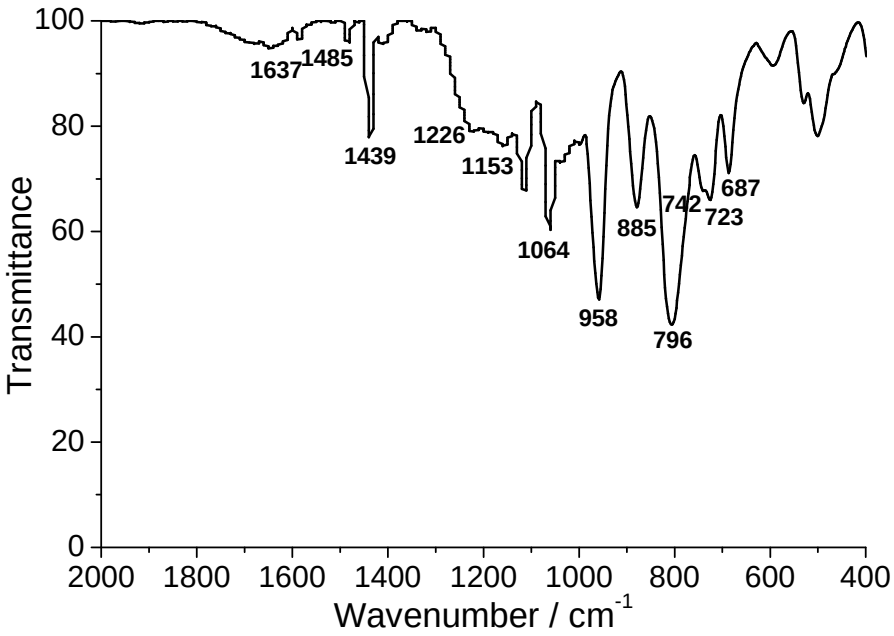

Figure S3-15. FT-IR of [**7**·H]$_3$[PMo$_{12}$O$_{40}$] on KBr Pellet. FT-IR (KBr, cm^{-1}): ν = 1637, 1485 (C=C), 723, 687 (C–H), 1439 (P–Ar), 742 (P–CH$_2$), 1226, 1153 (S=O), 1064 (P–O$_a$), 958 (Mo=O$_d$), 885 (W–O$_b$–W), 796 (W–O$_c$–W).

Figure S4. GC-MS analysis

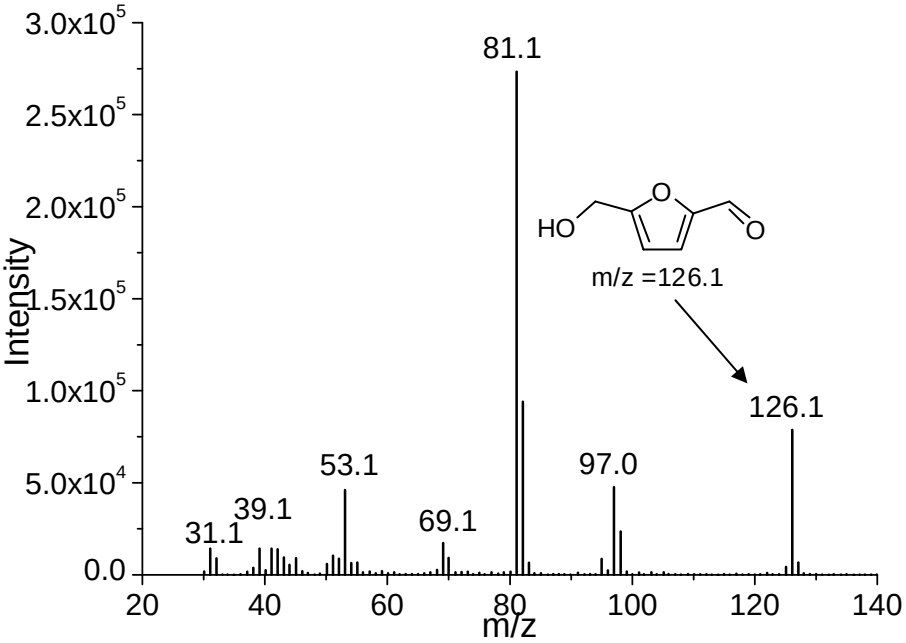

Figure S4-1. MS of 5-hydroxymethylfurfural

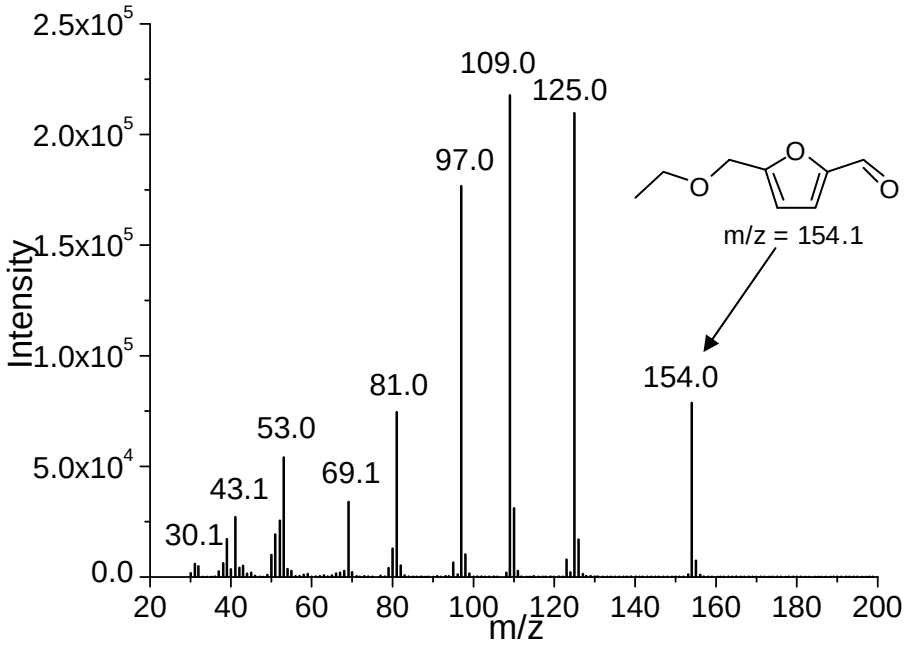

Figure S4-2. MS of 5-ethoxymethylfurfural

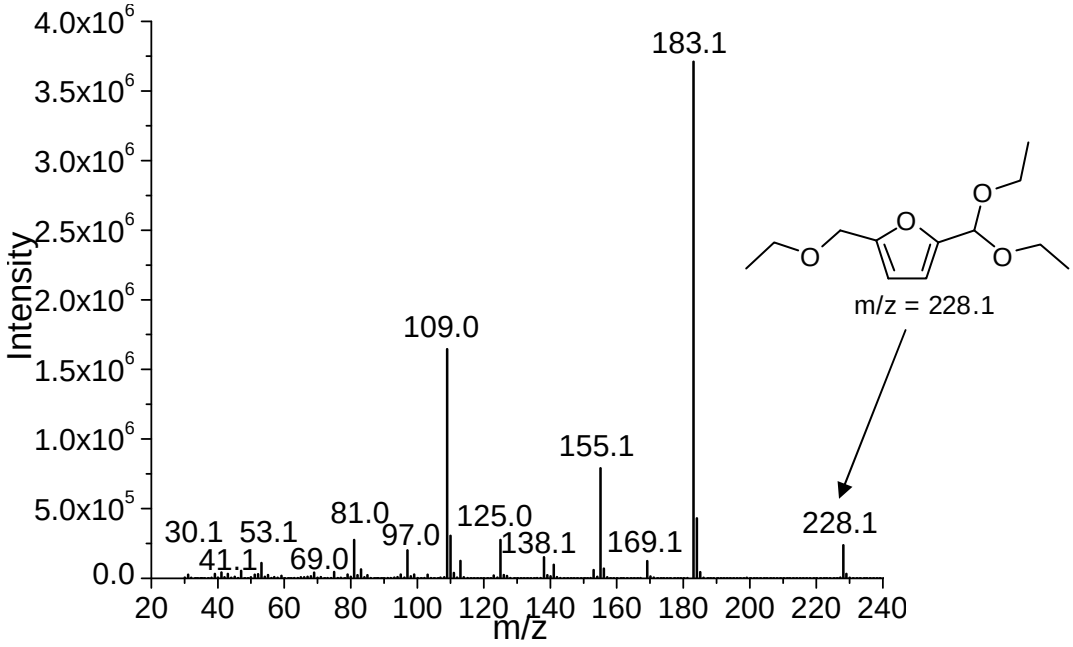

Figure S4-3. MS of 2-(diethoxymethyl)-5-(ethoxymethyl)furan

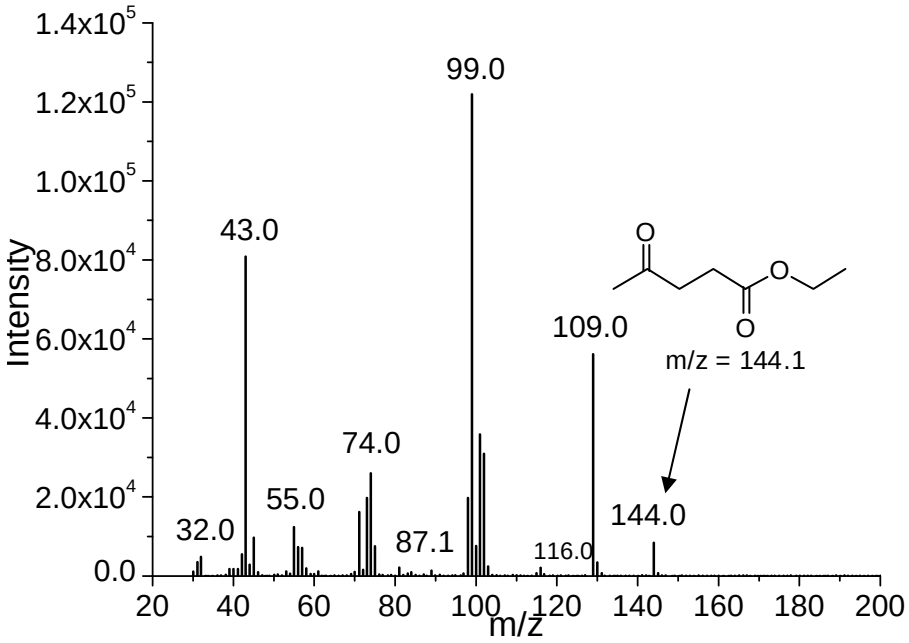

Figure S4-4. MS of ethyl levulinate

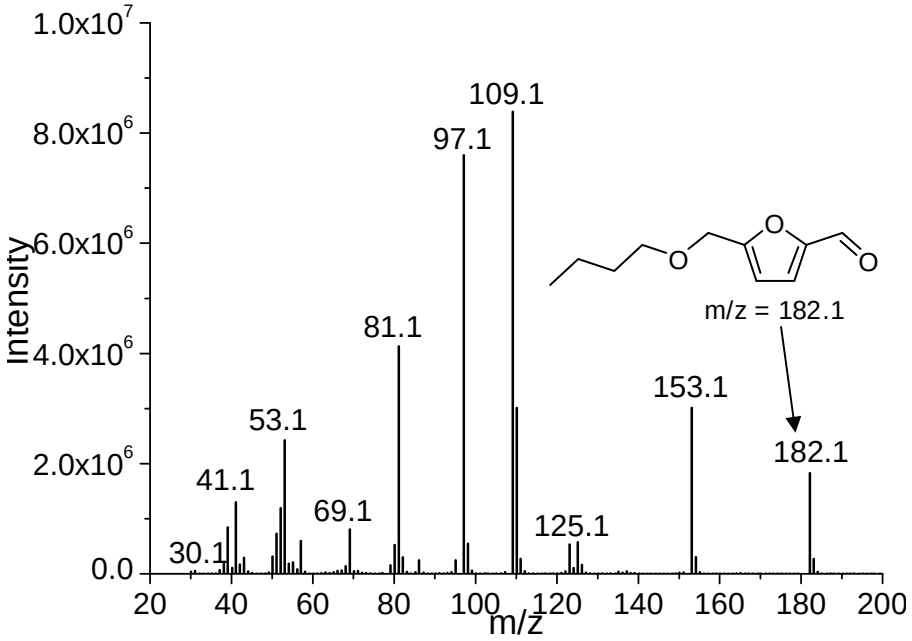

Figure S4-5. MS of 5- butoxymethylfurfural

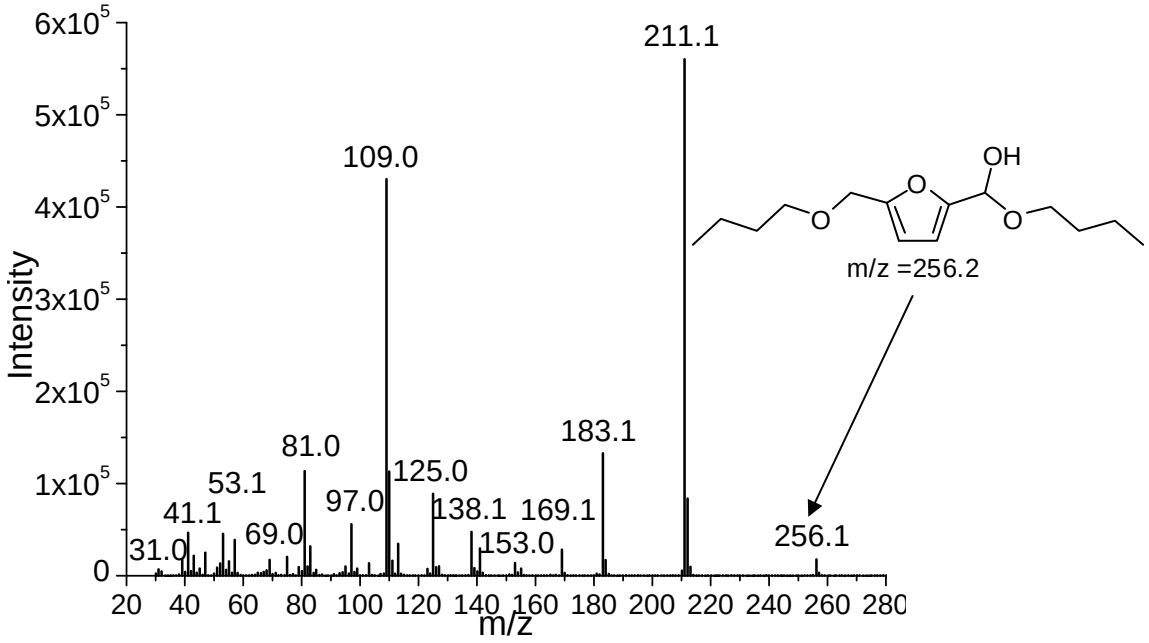

Figure S4-6. MS of 2-(1′-butoxymethyl-1′-hydroxyl)-5-(butoxymethyl)furan

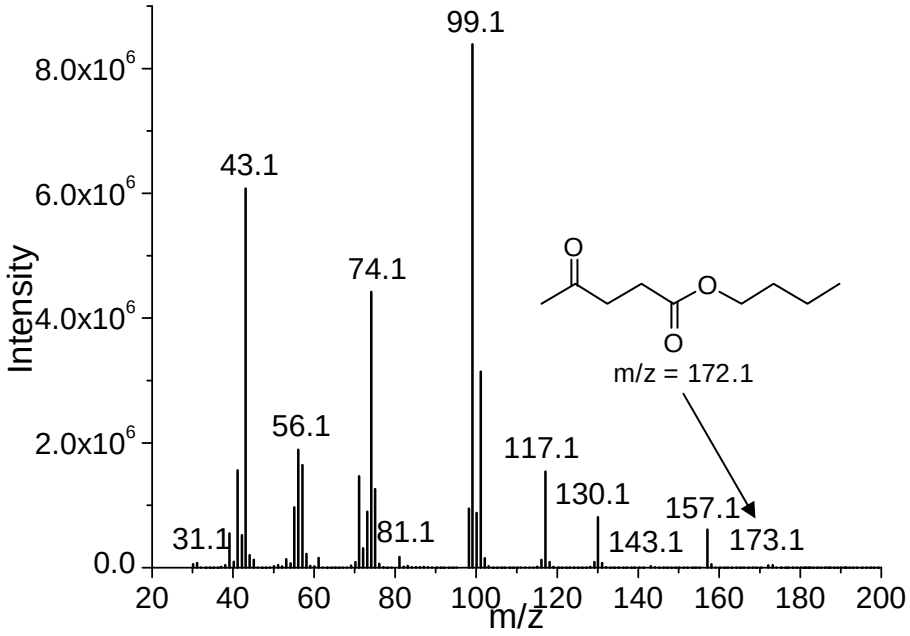

Figure S4-7. MS of butyl levulinate